Self-sustained pulsations in a quantum-dot laser

E. A. Viktorov[1,2] and T. Erneux[2]
[1]*National Research University of Information Technologies, Mechanics and Optics, Saint Petersburg, Russia*
[2]*Optique Nonlinéaire Théorique, Campus Plaine, CP 231, 1050 Bruxelles, Belgium*
(Received 30 April 2014; published 17 November 2014)

We analyze a delay differential equation for the amplitude of the electrical field in order to understand recent experimental observations of low-frequency oscillations in a QD laser. The laser contains no saturable absorber section and exhibits no relaxation oscillations. We investigate the problem both analytically and numerically. We show that there exists a homoclinic bifurcation from a cavity mode that is responsible for the generation of low-frequency pulsating oscillations. We discuss the role of optothermal effects in the formation of the pulsed dynamics.

DOI: 10.1103/PhysRevE.90.052914 PACS number(s): 05.45.−a, 42.55.Px, 42.65.Sf

Self-pulsing regimes in semiconductor lasers have been analyzed, experimentally and theoretically, for decades and continue to attract significant attention due to the strong impact of these instabilities on the laser performance and its applications [1]. The observation of pulsating intensity oscillations in the GHz range is conventionally attributed to saturable absorption (passive Q-switching). These self-sustained pulsations in bulk and quantum-well lasers are generated by the presence of saturable absorbing regions located outside the active region [2]. In order to explain the self-pulsations in quantum-dot (QD) lasers, the saturable absorption was assumed to be the result of inhomogeneous broadening of the gain and the existence of several confined QD states [3]. A recent experimental investigation of an InAs QD laser without a saturable absorber reported on large amplitude self-sustained pulsations in the MHz range [4]. The MHz range and the nonmonotonic change of the pulsation frequency with current exclude the passive Q-switching mechanism. The shape of each pulse corresponds to a sharp jump up, a slower decay, followed by a drop out. The slower decay is less pronounced at higher pumping currents. There is a jitter in the pulse width for the full range of pump currents. Due to limited information from the grower, we have no details on the material properties of the device, which operates strictly at the ground state (GS) transition.

QD-based semiconductor lasers offer several advantages for applications such as a low-threshold current, temperature stability, and small dynamical chirp [5]. Of particular interest is a high damping rate of the relaxation oscillations (ROs) compared to the ROs of lasers based on bulk and QW materials [6,7]. This implies a higher stability with respect to optical feedback [8] and optical injection [9]. Lasers free of ROs are known as "Class A lasers" and approach their equilibrium exponentially like an overdamped oscillator. By contrast, lasers known as "Class B lasers" exhibit slowly decaying ROs toward their steady state. Only one equation for the amplitude of the field is needed for Class A lasers while we need both the equation for the field and the equations for the material variables in the case of Class B lasers.

In this paper, we consider a mathematical model for a Class A laser that admits large amplitude self-sustained pulsations. The period of the oscillations is several orders larger than the laser cavity round-trip time. The profile of the pulse consists of a jump up, a slower decay, followed by a drop out that are reminiscent of the experimental time traces observed in Ref. [4]. Our objective is not to simulate the experiments reported in Ref. [4] but to determine from this model what bifurcation mechanism could lead to large period oscillations.

The absence of dominant RO oscillations in the experiments [4] motivates us to adiabatically eliminate all material variables in the laser rate equations and to consider only an equation for the normalized complex amplitude of the electrical field $E(t)$. A similar simplification has previously been exploited in Ref. [10]. From the rate equation models used to describe the response of mode-locked QD lasers [11,12], we find that $E(t)$ satisfies the following delay differential equation:

$$\gamma^{-1}E'(t)+E(t)=\sqrt{\kappa}\exp[(1-i\alpha)G(t-T) -i\phi(t-T)]E(t-T), \quad (1)$$

where prime means differentiation with respect to time t. The delay T is equal to the cold cavity round-trip time. The attenuation factor κ describes the total nonresonant linear intensity losses per cavity round-trip. The bandwidth of the spectral filtering is γ and the line-width enhancement factor in the gain is α. The variable $G(t)=J(1+|E(t)|^2)^{-1}$ is the time-dependent dimensionless cumulative saturable gain, where J is the pump parameter. The phase ϕ takes into account a possible detuning of the frequency of the gain maximum from the optical frequency of the closest cavity mode and is determined by the cavity length. It defines the relative location of the filter and the nearest mode in the case of narrow filtering [11]. Its variation in time accounts to the thermal change of the refractive index.

We first consider Eq. (1) with $\phi(t)=\phi_0$ (no optothermal effects) and determine the bifurcation diagram of the stable solutions in terms of ϕ_0. We then explore the effect of a slowly varying $\phi(t)$. To this end, we introduce the dimensionless time $s\equiv t/T$ into Eq. (1) and obtain

$$\Gamma^{-1}E'+E=\sqrt{\kappa}\{\exp[(1-i\alpha)G(s-1)-i\phi_0]\}E(s-1), \quad (2)$$

where prime now means differentiation with respect to time s. $\Gamma\equiv\gamma T$ is the product of the round-trip time and the bandwidth of the spectral filtering. It is an important parameter because it controls the number of cavity modes (CMs). The CMs are defined as the solutions of Eq. (2) of the form

$E = R\exp(i\omega s)$. From Eq. (2), we find that R and ω satisfy the two conditions:

$$1 = \sqrt{\kappa}\exp(G)\cos(\alpha G + \phi_0 + \omega), \tag{3}$$

$$\Gamma^{-1}\omega = -\sqrt{\kappa}\exp(G)\sin(\alpha G + \phi_0 + \omega), \tag{4}$$

where

$$G = \frac{J}{1+R^2}. \tag{5}$$

Eliminating the trigonometric functions in Eqs. (3) and (4) leads to an expression for $G = G(\omega)$ of the form

$$G = \tfrac{1}{2}\ln\{[1 + (\Gamma^{-1}\omega)^2]/\kappa\}. \tag{6}$$

By eliminating $\sqrt{\kappa}\exp(G)$ in Eqs. (3) and (4), we obtain

$$\tan(\alpha G + \phi_0 + \omega) = -\Gamma^{-1}\omega. \tag{7}$$

Together with the condition

$$\cos(\alpha G + \phi_0 + \omega) > 0 \tag{8}$$

coming from Eq. (3), Eq. (7) provides ϕ_0 as

$$\phi_0 = -\alpha G - \omega - \arctan(\Gamma^{-1}\omega) + n\pi, \tag{9}$$

where $n = 0$, is an integer.

We examine Eq. (2) for small $\Gamma = 0.375$. The bifurcation diagram of the CMs is then determined in the following way. We gradually change ω, determine G from Eq. (6), then R^2 from Eq. (5) and finally the value of the bifurcation parameter ϕ_0 using Eq. (9). Figure 1 displays the CM branches for $n = 0$ and $n = 2$ in the range $0 < \phi_0 < \pi$. The CM branch

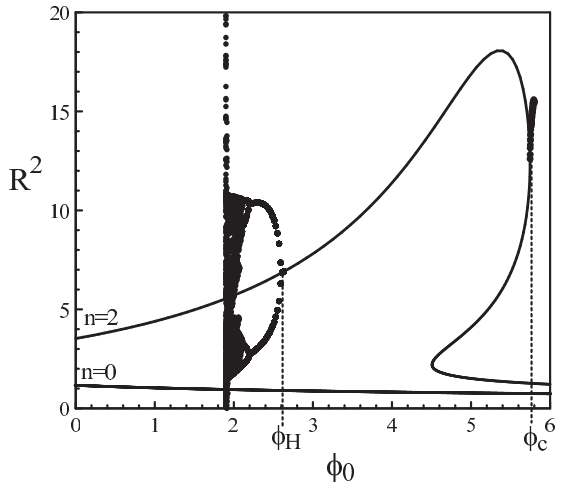

FIG. 1. Bifurcation diagram of the CMs $n = 0$ and $n = 2$ in the interval $0 < \phi_0 < 2\pi$. ϕ_H and ϕ_c denote a Hopf bifurcation point and a homoclinic bifurcation point, respectively. As $\phi_0 - \phi_H$ progressively decreases from zero, stable oscillations appear and the figure represents the extrema determined numerically. As $\phi_0 - \phi_c$ increases from zero, a branch of periodic solutions emerges with a large period. The figure represents the time-average of R^2 obtained numerically. The values of the fixed parameters are $\Gamma = 0.375$, $J = 7$, $\kappa = 0.48$, and $\alpha = 2.5$.

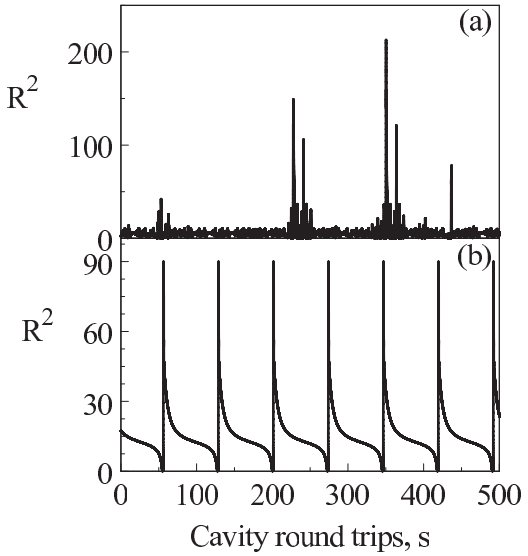

FIG. 2. Numerical time traces: (a) bursts of spiking oscillations for $\phi_0 = 1.9$ (b) large amplitude periodic oscillations for $\phi_0 = -0.5$ (or $\phi = 5.78$).

for $n = 0$ is the same as the one for $n = 2$ but shifted to the left by a factor 2π in ϕ_0. More precisely, the permitted CM branches have the same profile with a maximum located at $\phi_0 \simeq 5.2 + (n-2)\pi$, where $n = 0, \pm 2, \pm 4, \ldots$ Overlaps of low amplitude tails are thus possible but seem not to play a role for the narrow bandwidth filtering ($\Gamma = 0.375$). There are two important bifurcations from the $n = 2$ branch located at ϕ_H and ϕ_c. The laser operates at a stable steady state only in the the interval $\phi_H < \phi_0 < \phi_c$. A supercritical Hopf bifurcation appears at $\phi_0 = \phi_H$, and Fig. 1 shows the extrema of the oscillations as we progressively decrease ϕ_0 from ϕ_H. After a series of period-doubling bifurcations and a weak chaos, the amplitude of the oscillations dramatically increases to high values near $\phi_0 = 1.93$. The response of the laser then takes the form of large amplitude bursts of spiking oscillations [see Fig. 2(a)]. As we further decrease ϕ_0, regular large amplitude periodic oscillations progressively appear [see Fig. 2(b)]. By contrast to the oscillations near the Hopf bifurcation point, they are strongly pulsating in time and the period is much larger. As we progressively approach $\phi_0 = \phi_c - 2\pi$ (or equivalently, $\phi_0 = \phi_c$), the interpulse period increases. The period becomes infinite at the homoclinic bifurcation point located at $\phi_0 = \phi_c$. It corresponds to the coordinate of the CM limit point where the period of the oscillations becomes infinite. The time average of the oscillations approaches a constant equal to $R_c^2 = R^2(\phi_c)$ (see Fig. 3). Because the interval between pulses is the essential contribution to the period and because R^2 remains close to R_c^2, we may consider the normal form equation (which coincides with the normal form of a saddle-node bifurcation [1]) for the CM limit point as a fair description of the interpulse stage. The slow time is scaled by the square root of the deviation from the limit point, which means that period P of the interpulse stage increases like

$$P \sim (\phi_0 - \phi_c)^{-1/2} \tag{10}$$

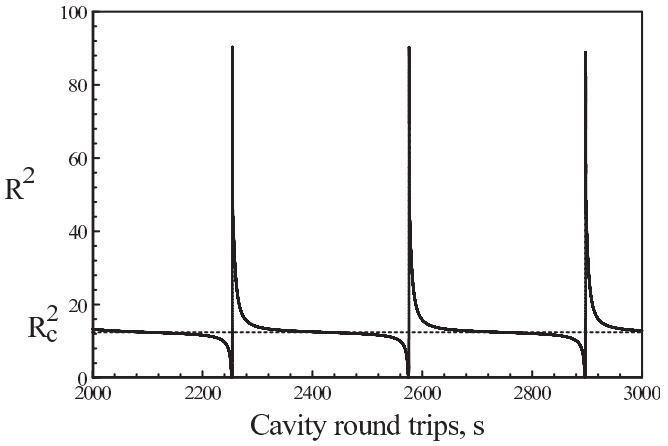

FIG. 3. Time trace of low-frequency large-amplitude pulsations for $\phi_0 = 5.748$. R_c^2 corresponds to the CM limit point described in the legend of Fig. 1.

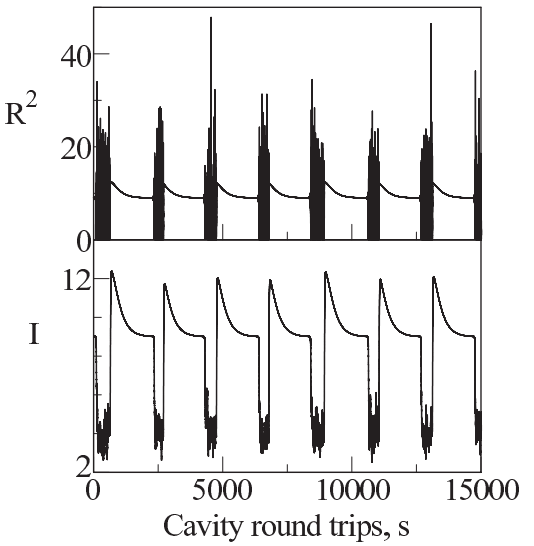

FIG. 4. Unfiltered (a) and filtered (b) time traces of low-frequency large-amplitude pulsations. $\gamma_{\text{th}} = 0.001$; $\phi_0 = 4$; $\beta = 0.8$ and $\Gamma = 3$, $J = 5$, $\tau_f = 10$. The other parameters remain the same as described in the legend of Fig. 1.

as $|\phi_0 - \phi_c| \to 0$. In the bifurcation diagram (Fig. 1), the branching of these periodic solutions from $\phi_0 = \phi_c$ is shown by their numerically computed time averages.

The experimentally observed low-frequency pulsations were reasonably attributed to optothermal effects [4]. It is a scenario that has been theoretically examined for semiconductor etalon [13] and reported for semiconductor optical amplifiers [14,15]. Our bifurcation diagram confirms this hypothesis: the laser output changes dramatically if the phase ϕ varies in the vicinity of the homoclinic bifurcation point. In our system, the phase variations are directly related to the cavity variations caused by the optothermal coupling. In order to describe the evolution of ϕ, we introduce

$$\gamma_{\text{th}}^{-1}\phi'(s) = -\phi + \phi_0 + \beta|E|^2, \tag{11}$$

where γ_{th} is the slow thermal relaxation rate with $\gamma_{\text{th}} \ll \Gamma$. ϕ_0 is the phase in the absence of the optothermal effects, and β is an amplitude of the thermal index change and the control parameter. Similar to Ref. [15], we assume that the effective index and the phase ϕ depend linearly on temperature. In order to match the experimental results, we have filtered the time series. The filtered intensity I is determined by

$$I' = (|E|^2 - I)/\tau_f, \tag{12}$$

where τ_f is the time constant of the filter. Numerical results are shown in Fig. 4 for $\Gamma = 3$. The filtered time trace is very similar to the experimental traces in Ref. [4] and consists of the trapezoidal intensity pulses separated by low-intensity states. The lower-intensity state corresponds to the fast-amplitude fluctuations of R^2 in Fig. 4(a). These fluctuations occur on the timescale of the cavity round-trips ($s = t/T$) and are, therefore, much faster than the slow-pulsed dynamics, which corresponds to the MHz range for a 3.5-mm cavity length in Ref. [4].

This time scale represents the coupling between individual lasing modes. A possibility of the coupling has been predicted by the analysis of low-amplitude tails for $\phi(s) = \phi_0$ case with narrow filtering $\Gamma = 0.375$ and becomes strongly pronounced for broader filtering $\Gamma = 3$, which corresponds to a multimode operation. Experimental dynamics of the individual modes remain unrevealed in Ref. [4], and we do not explore the fast-amplitude fluctuations in detail.

In this paper, we considered a Class A laser delay differential equation for the complex amplitude of the electrical field that does not admit ROs. This equation is derived from a rate equation model that has been previously used to explore the stability of a mode-locked QD laser. Our equation is still strongly nonlinear, but the fact that it is in terms of only one dependent variable allows combined analytical and numerical studies of the bifurcation diagram. We show that low-frequency oscillations are possible and result from a homoclinic bifurcation from a specific mode cavity. We then demonstrate that by taking into account the slow changes of the phase due to optothermal effects, we obtain time traces that are in excellent qualitative agreement with the experimental observations.

The authors acknowledge the support of the Fonds National de la Recherche Scientifique (Belgium) and the Belgian Science Policy Office under Grant No. IAP-7/35 "photonics@be."

[1] T. Erneux and P. Glorieux, *Laser Dynamics* (Cambridge University Press, Cambridge, UK, 2010).

[2] M. Yamada, IEEE J. Quantum Electron. **29**, 1330 (1993).

[3] S. Mokkapati, H. H. Tan, C. Jagadish, and M. Buda, Appl. Phys. Lett. **92**, 021104 (2008).

[4] A. Tierno, N. Radwell, and T. Ackemann, Phys. Rev. A **84**, 043828 (2011).

[5] D. Bimberg, M. Grundmann, and N. N. Ledentsov, *Quantum Dot Heterostructures* (Wiley, New York, 1999).
[6] T. Erneux, E. A. Viktorov, and P. Mandel, Phys. Rev. A **76**, 023819 (2007).
[7] K. Lüdge, M. J. P. Bormann, E. Malic, P. Hövel, M. Kuntz, D. Bimberg, A. Knorr, and E. Schöll, Phys. Rev. B **78**, 035316 (2008).
[8] D. O'Brien, S. P. Hegarty, G. Huyet, and A. V. Uskov, Opt. Lett. **29**, 1072 (2004).
[9] T. Erneux, E. A. Viktorov, B. Kelleher, D. Goulding, S. P. Hegarty, and G. Huyet, Opt. Lett. **35**, 937 (2010).
[10] D. Pieroux and Paul Mandel, Phys. Rev. E **68**, 036204 (2003).
[11] A. G. Vladimirov and D. Turaev, Phys. Rev. A **72**, 033808 (2005).
[12] E. A. Viktorov, P. Mandel, A. G. Vladimirov, and U. Bandelow, Appl. Phys. Lett. **88**, 201102 (2006).
[13] Y. A. Rzhanov, H. Richardson, A. A. Hagberg, and J. V. Moloney, Phys. Rev. A **47**, 1480 (1993).
[14] S. Barland, O. Piro, M. Giudici, J. R. Tredicce, and S. Balle, Phys. Rev. E **68**, 036209 (2003).
[15] F. Marino, G. Catalán, P. Sánchez, S. Balle, and O. Piro, Phys. Rev. Lett. **92**, 073901 (2004).